

Article

Microstructure and Mechanical Properties of Ti6Al4V Alloy Consolidated by Different Sintering Techniques

Doan Dinh Phuong^{1,2}, Luong Van Duong^{1,2} , Nguyen Van Luan^{1,2}, Nguyen Ngoc Anh¹ and Pham Van Trinh^{1,*} 

¹ Institute of Materials Science, Vietnam Academy of Science and Technology, 10072 Hanoi, Vietnam; phuongdd@ims.vast.ac.vn (D.D.P.); duonglv@ims.vast.ac.vn (L.V.D.); luannv@ims.vast.ac.vn (N.V.L.); anhnn@hus.edu.vn (N.N.A.)

² Graduate University of Science and Technology, Vietnam Academy of Science and Technology, 10072 Hanoi, Vietnam

* Correspondence: trinhpv@ims.vast.vn; Tel.: +849-4319-0301

Received: 13 August 2019; Accepted: 21 September 2019; Published: 23 September 2019



Abstract: In this paper, we investigated the effect of the different sintering techniques including vacuum sintering, capsule-free hot isostatic pressing (HIP), and capsule HIP on the microstructure and mechanical properties of Ti6Al4V alloy. The obtained results indicated that full density Ti6Al4V alloy could be obtained by using capsule HIP technique. The alloy sintered by capsule HIP had the highest hardness (~405 HV) and compressive yield strength (~1056 MPa). It is interesting that the geometry has a significant influence on the relative density and mechanical properties of the alloy sintered by the capsule-free HIP. The relative density, hardness, and compressive yield strength rise from center to periphery of the specimen. This is attributed to the heating and pressing in the capsule-free, which are external, leading to the densification processes starting from the outside to the inner parts of the pressed specimen. Using theoretical prediction with Gibson and Ashby power law found that the yield strength of the alloy sintered by capsule-HIP technique is much lower than that of the calculated value due to the formation of the coarse lamellar microstructure of α -Ti grains.

Keywords: sintering; hot isostatic pressing; Ti6Al4V and microstructure; mechanical properties

1. Introduction

Ti6Al4V alloy has exhibited unique properties such as high specific strength, excellent fracture toughness, excellent corrosion resistance, and good biocompatibility. Ti6Al4V alloy has been widely used in many industry sectors such as automobile, aerospace, and biomedical [1,2]. In fact, Ti6Al4V alloy has demonstrated the significant improvement both in the energy efficiency and in the lifetime of the specific components due to their own lightweight and high strength. Two conventional methods including forging and casting are used to fabricate the titanium or titanium alloy based components. The casting is more commonly used in comparison with the forging due to the high potential process of the complex structural components and high utilization of raw materials [3,4]. The powder metallurgy (PM) techniques such as vacuum sintering, hot isostatic pressure (HIP), channel angular pressure, and spark plasma sintering (SPS) have been widely using to fabricate the dense and porous Ti6Al4V components [5–12]. Up to now, many studies have been done to find the best technique to fabricate Ti6Al4V. Beside of these conventional techniques, some new technologies have been developed for manufacturing the Ti alloys such as selective laser melting (SLM) and electron beam melting (EBM). Although considered as the innovative industrial production technologies, they have not been widely used compared to the conventional techniques due to the complicated and expensive equipment [13,14]. Compared to the new technologies, the conventional

PM techniques usually cause some disadvantages such as porosity and composition segregation, which reduce the mechanical properties of the components and difficult to be removed during the fabrication process [10–12]. Many studies have focused on controlling the porosity (shape, size, and volume fraction) and the microstructures problems like martensitic microstructures and/or shape and size of $\alpha+\beta$ phases by changing some sintering parameters such as heating rate, particle size, pressure, and temperature [15–17]. Xu and Nash [18] have studied the effect of the heating rates on the Ti6Al4V alloy sintered by vacuum sintering. The obtained results demonstrated the densification is driven by the lattice diffusion mechanism. Cabezas-Villa et al. investigated the mechanical properties of Ti6Al4V powders with different particle sizes [19]. Recently, HIP technique has been extensively utilized to fabricate Ti6Al4V alloy in a wide range of industries due to the possibility in producing complex shape, fully dense components, and the potential economic advantages [20–23]. Delo and Piehler [24] proposed the sintering model during HIP with early stage of Ti6Al4V powder compacts. Zhang et al. [25] investigated the effect of the temperature on the microstructure and mechanical properties of Ti6Al4V alloy. Xu et al. studied the effect of the cooling rate on microstructure and properties of Ti6Al4V alloy from atomized powder [11]. Most of the previous studies on Ti6Al4V mainly focus on the effect of the sintering parameters on the microstructure and mechanical properties of the alloy sintered by a specific sintering technique. At present, there are no comparative studies on the effect of different sintering techniques on the microstructure and mechanical properties of Ti6Al4V alloy.

Thus, this work investigates the effect of the different sintering techniques including vacuum sintering, capsule-free HIP, and capsule HIP on the microstructure and mechanical properties of Ti6Al4V alloys. The microstructure was characterized by scanning electron microscopy and optical microscopy method. The mechanical properties were evaluated through hardness and compression tests on the different positions of the sintered specimens.

2. Materials and Methods

The consolidation process of Ti6Al4V alloy by different sintering techniques including vacuum sintering, capsule-free HIP, and capsule HIP is shown in Figure 1. For vacuum sintering, commercial Ti6Al4V alloy powder with an average particle size of 45 μm (Figure 2a), supplied by Kiswel Co. Ltd. (Seoul, Korea) was compacted in a cylindrical mold to obtain pellets with 12 mm in height and 22 mm in diameter under a load of 200 MPa for 5 s. The obtained pellets were sintered in a vacuum furnace at 1100 °C with a heating rate of 10 °C/min for 3 h in vacuum ($\sim 2 \times 10^{-3}$ Pa) then cooling down to room temperature. For capsule-free HIP, the capsule-free HIP (AIP6-30 H, American Isostatic Presses Inc, Ohio, USA) were used to reconsolidate the vacuum sintered Ti6Al4V alloy specimens. The specimens were put in the chamber and heated (10 °C/min) up to 1100 °C, then holding for 2 h dwell after that applying the pressing process under a load of 100 MPa for 15 min at this temperature to obtain the capsule-free HIP samples. For capsule HIP, Ti6Al4V alloy powders were first filled into cylindrical low carbon steel containers with a size of 22 mm in diameter and 15 mm in height, then degassed at 300 °C for 3 h at 10^{-3} Pa vacuum level. The sealed powders were introduced in the HIP chamber then heated at 1100 °C under vacuum. The temperature of 1100 °C was kept for 2 h and followed by 15 min pressing with a load of 100 MPa to obtain the capsule HIP samples. The specimens sintered by three different techniques were cut and polished down to a shape of 10 mm in height and 20 mm in diameter as shown in Figure 2b.

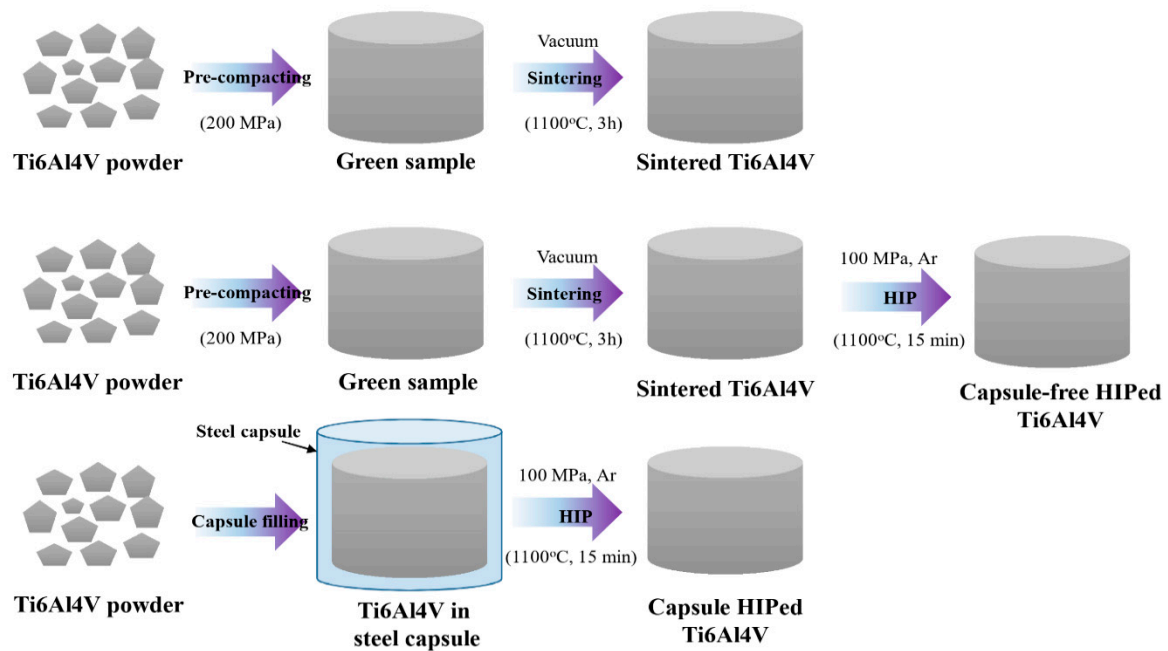


Figure 1. Fabrication process of Ti6Al4V alloys consolidated by different sintering techniques.

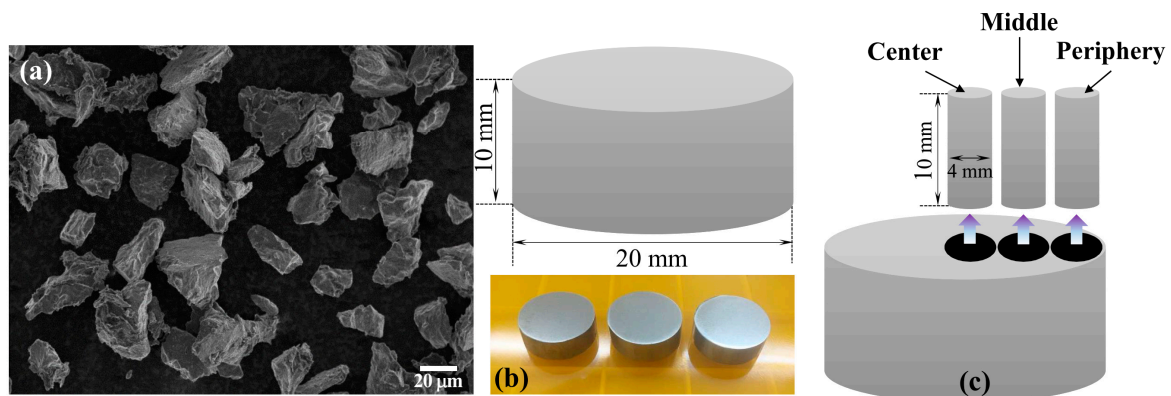


Figure 2. (a) SEM image of Ti6Al4V powder, (b) optical picture of Ti6Al4V alloy after sintering, and (c) schematic of cutting process for the test specimen.

The testing samples were selected at three positions including periphery, middle, and center of the sintered specimens to investigate the effect of geometry on the microstructure and mechanical properties of the sintered specimens. The cylindrical samples cut out from the periphery, middle, and center of the specimen by using a wire-cutting machine. The schematic of the cutting process for the test samples with 4 mm in diameter and 10 mm in height is shown in Figure 2c. The phase compositions of the sintered specimens were recorded by the X-ray diffraction technique using an ARL EQUINOX 1000 X-ray diffractometer equipped with $\text{CuK}\alpha$ radiation. The specimens were polished and then etched with Kroll's reagent (3 mL HF + 6 mL HNO_3 + 100 mL H_2O) to observe the microstructure by using a field emission scanning electron microscopy (FESEM, Hitachi S4800, Hitachi, Tokyo, Japan) and an optical microscope (OM, Axiovert 40MAT, Carl Zeiss, Germany). The 2D apparent pore size was measured using image analysis software (ImagePartnerTM; Saramsoft Co. Ltd., Gyeonggi-do, Korea). The density of the sintered specimens was measured using the Archimedes method. The hardness was measured by a Vickers hardness tester (AVK-CO, Mitutoyo, Kawasaki, Japan) under a load of 9.8 N for 10 s. The compressive tests were performed on cylindrical specimens with 4 mm in diameter and 8 mm in height using a universal testing machine (Tinius Olsen Super L120) at a speed of 0.5 mm/min at room temperature. The reported values on the relative density, hardness, and compressive strength

represent the average of five measurements at the same conditions in order to ensure the repeatability of experimental data.

3. Results

3.1. Microstructure and Phase Compositions

The microstructure of the specimens sintered by vacuum sintering, capsule-free HIP, and capsule HIP was investigated by SEM and OM. Figure 3 shows the microstructure of the specimen sintered by vacuum sintering at different positions from center to periphery. The microstructure is nearly the same at all positions of the specimens. Many pores with a size of 50 μm were observed and thus implied the low densification of the specimens. Figure 4 shows the microstructure of the specimen sintered by the capsule-free HIP. From the figure, many pores at the center of the specimen and few pores at the periphery of the specimen are observed. The pore size was measured to be 50 μm , 31 μm , and 15 μm corresponding to center, middle, and periphery position of the specimens, respectively. The decrease of the pore size from center to periphery position demonstrated that the densification progressively increased from the periphery to the center of the specimen. This could be explained by the effect of non-uniform forces caused a gradient in specimen densification. Indeed, the heating and pressing in the capsule-free are the external processes resulting in the densification beginning from the outside then progressively affecting the inner parts of the pressed specimen. The outer shell formed during the first step screened inner parts from high pressure, and thus grains at the center and middle position were subjected to lower pressures than the grains at periphery position [26]. Besides, the gas holes possibly formed at the center of the specimen during the pre-compacting, and vacuum sintering process could not be removed during the capsule-free HIP process due to the formation of the outer shell. This is why the pore size at the center is much larger than that of the periphery position. Figure 5 shows the microstructure of the specimen sintered by capsule HIP technique. No pores could be observed on the polished surface at all positions of the specimens that implied the good densification of the specimen. The obtained results demonstrated that Ti6Al4V alloy could reach to full density by using capsule HIP technique.

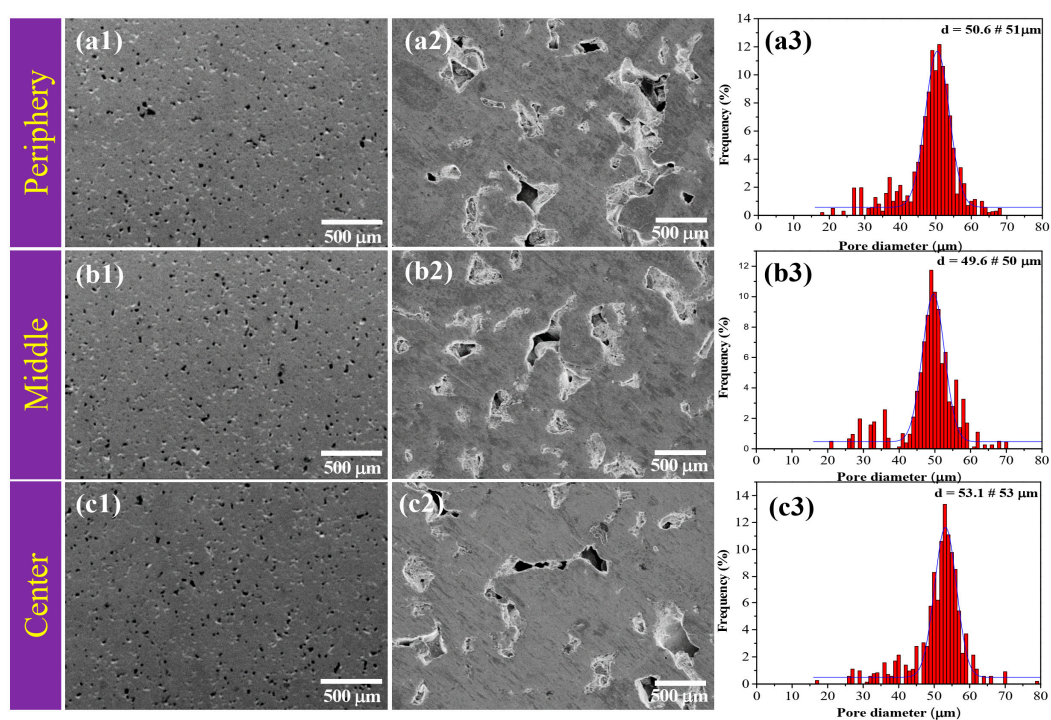


Figure 3. SEM images and pore size distribution of Ti6Al4V alloy sintered by vacuum sintering at different positions: (a1, a2, a3) periphery, (b1, b2, b3) middle, and (c1, c2, c3) center of the specimen.

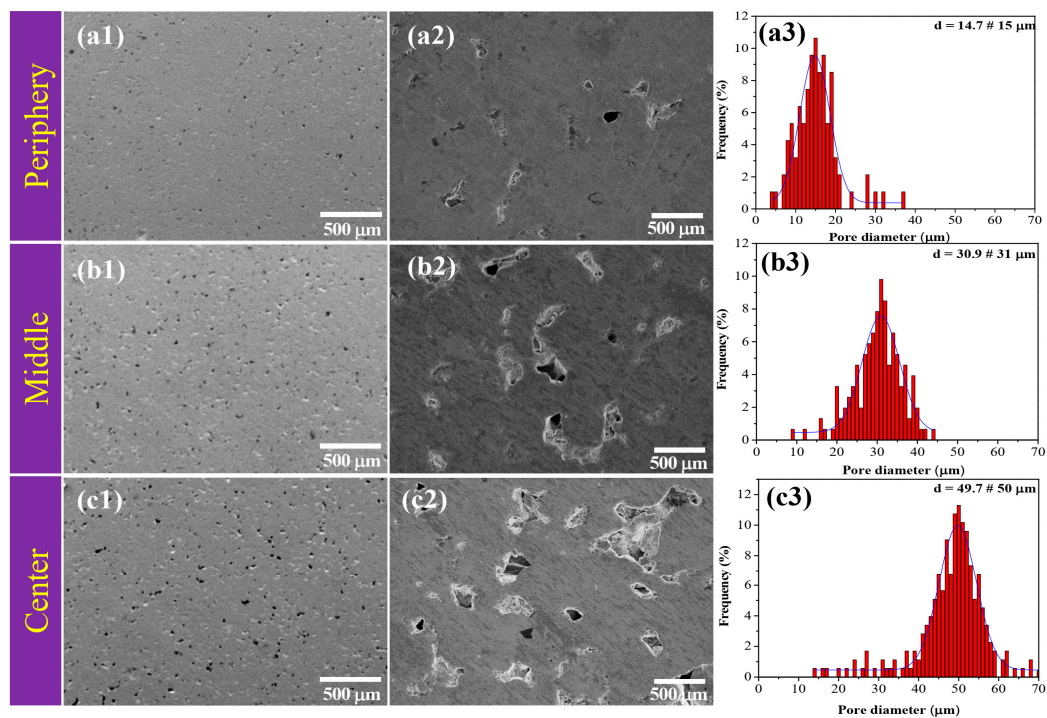


Figure 4. SEM images and pore size distribution of Ti6Al4V alloy sintered by capsule-free at different positions: (a1, a2, a3) periphery, (b1, b2, b3) middle, and (c1, c2, c3) center of the specimen.

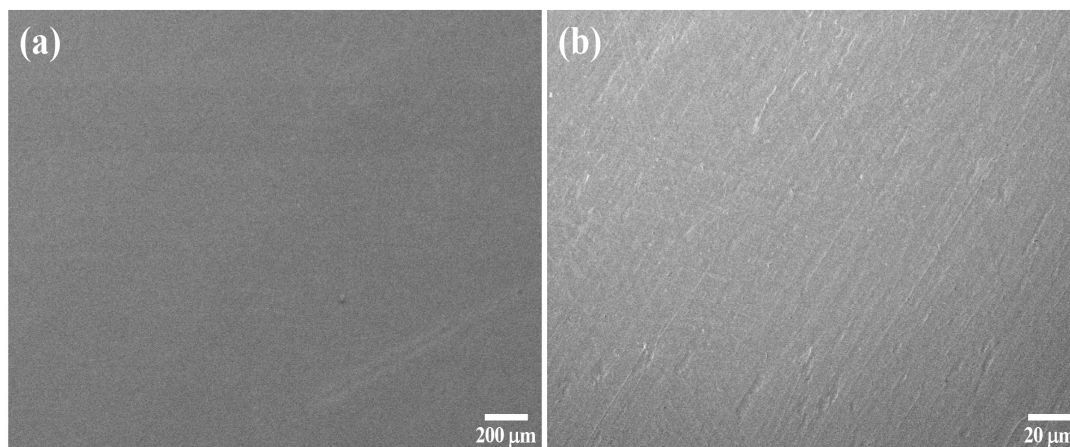


Figure 5. SEM images of Ti6Al4V alloy sintered by capsule hot isostatic pressing (HIP) at (a) low and (b) high magnification.

Figure 6 shows the microstructure at the center position of the Ti6Al4V alloys sintered by three different techniques. As can be seen, some pores (black area) were observed with the specimen sintered by vacuum sintering and capsule-free HIP. The $\alpha + \beta$ lamellar microstructure was observed for all specimens. The lamellar exists in both perpendicular and parallel forms. It is difficult to measure the columnar grain size due to grain boundary is hard to identify. However, it is clear that the size of α -Ti grains of the specimen sintered by capsule-free HIP is larger than that of the specimens sintered by vacuum sintering and capsule HIP. The coarse lamellar microstructure of α -Ti in case of the capsule-free HIP may negatively affect to the mechanical properties of the specimen.

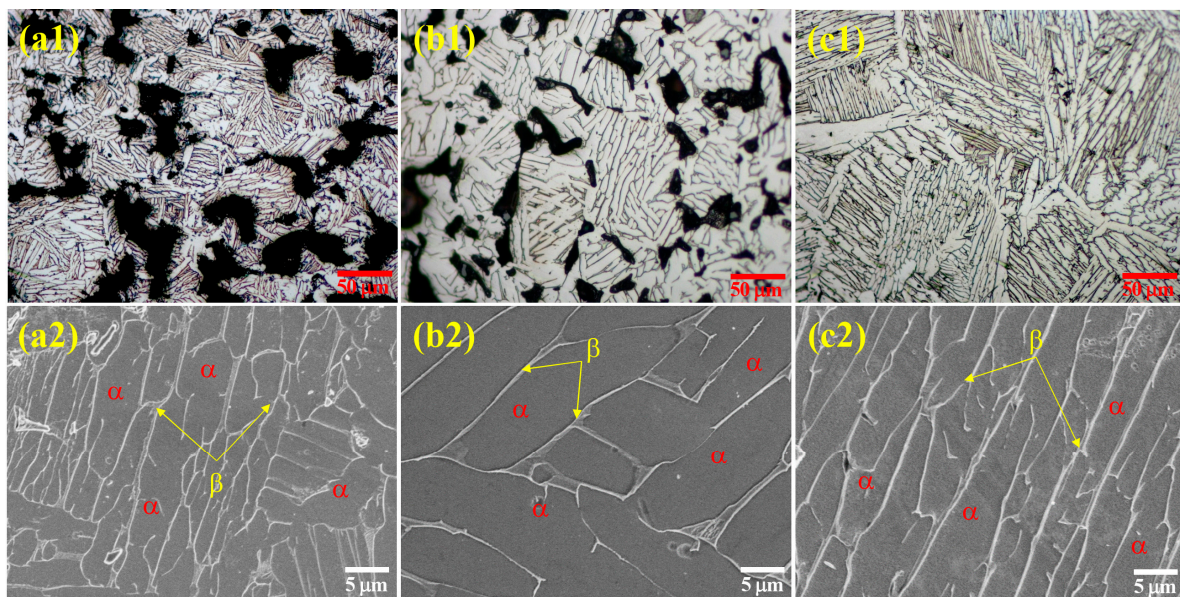


Figure 6. Microstructure of Ti6Al4V alloy sintered by different sintering techniques: (a1, a2) vacuum sintering, (b1, b2) capsule-free HIP, and (c1, c2) capsule HIP.

The phase composition of the sintered specimens observed by metallographic was confirmed by XRD. XRD patterns of the specimens are shown in Figure 7. As can be seen, for all specimens, some typical peaks of α -Ti at $2\theta = 35.15^\circ$, 38.72° , and 40.26° , corresponding to the (100), (002), and (101) plane, and β -Ti peak at 39.45° , corresponding to the (002) plane, respectively, were detected. The obtained results confirmed that the $\alpha + \beta$ microstructure of the specimens sintered by the different sintering techniques are in agreement with the microscopy observation as discussed earlier. Besides, there are no new phases which resulted from the reaction of the carbon steel container with Ti6Al4V alloy powder were detected at all positions from center to periphery of the alloy sintered by capsule HIP. This implied that the effect of interstitial elements and the effect of the dissolution of the carbon steel container during the capsule HIP process on the microstructure and mechanical behavior could be ignored.

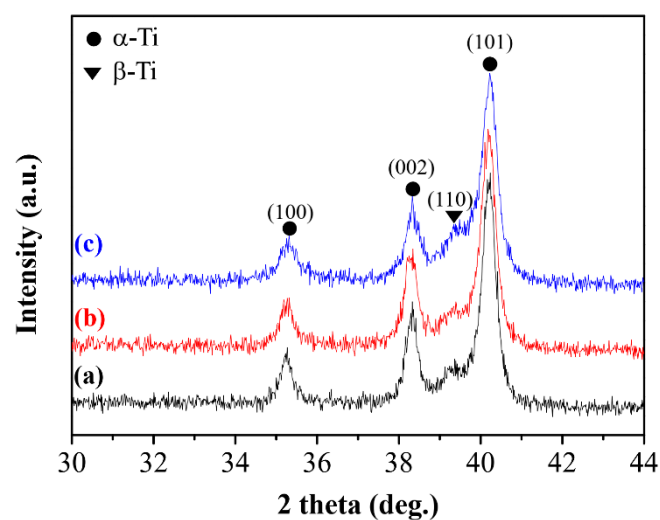


Figure 7. XRD patterns of Ti6Al4V alloy consolidated by vacuum sintering (a), capsule-free HIP (b), and capsule HIP (c).

3.2. Mechanical Properties

Figure 8 shows the relative density of Ti6Al4V alloy sintered by different sintering techniques versus different positions of the specimens. As can be seen, the relative density of the specimen sintered by vacuum sintering at the different positions is nearly the same of about 84%. Similarly, the specimens sintered by capsule HIP have the relative density in the range from 99.2% to 99.81% at different positions. In contrary, the relative density of the specimens sintered by capsule-free HIP is different from the center to the periphery position. The relative density increases from the center (85%) to periphery (96%) of the specimen. The change of the relative density versus different positions is consistent with the difference in the microstructure of the specimens sintered by capsule-free HIP. At the center, many pores with large size are observed that indicated the low densification. In contrary, the size of the pores at the periphery area is smaller, which implied the higher densification and thus improved the relative density of the specimens. The relative density of the specimens consolidated by vacuum sintering and capsule HIP is nearly similar in all positions as resulted from the uniform microstructure of the specimen. In conclusion, the capsule-free HIP has little contribution to relative density due to low densification at the center of the specimens; meanwhile, the specimen can reach full density by using capsule HIP technique.

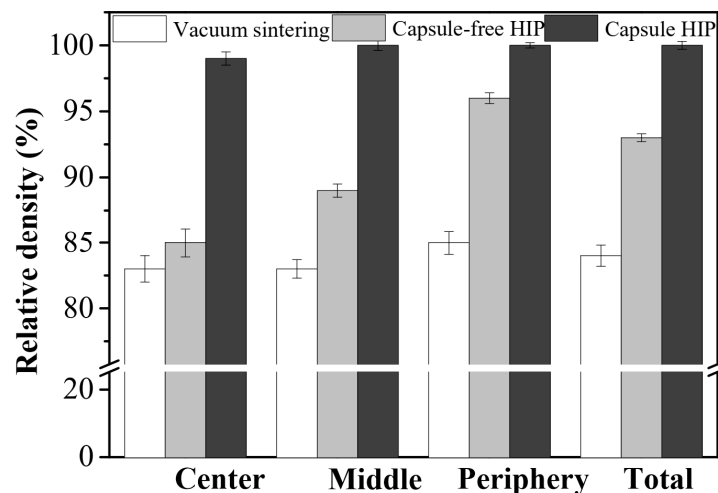


Figure 8. Relative density of Ti6Al4V alloy sintered by different sintering techniques versus different positions of the specimens.

Figure 9 shows the hardness of Ti6Al4V alloy sintered by different sintering techniques versus different positions of the specimens. As can be seen, the hardness of the specimens sintered by capsule HIP and vacuum sintering is nearly the same in all area. The specimens consolidated by capsule HIP has the highest hardness (~405 HV) that is 2.2 times higher than that of the specimens sintered by vacuum sintering. In contrary, the hardness of the specimens sintered by the capsule-free HIP is not the same at the different positions. The hardness is about 197 HV at the center, then increases to 285 HV at the middle area, and finally reaches up to 334 HV at the periphery of the specimens. The change in the hardness of the specimens sintered by capsule-free HIP could be due to the difference in the microstructure and the relative density as discussed in the previous sections.

Figure 10a–c shows the stress-strain compression curves at the middle position of Ti6Al4V alloy sintered by different techniques. The yield strength was measured to be 575 MPa, 628 MPa, and 1056 MPa, corresponding to the specimens sintered by vacuum sintering, capsule-free HIP, and capsule HIP, respectively. This means the specimens sintered by capsule HIP having the highest yield strength, which is nearly 1.85 times and 1.68 times higher compared to that of the specimens sintered by vacuum sintering and capsule-free HIP. The obtained results are consistent with the hardness and relative density of the specimens. The specimens with higher relative density have higher mechanical

properties. The effect of geometry on the compressive strength was investigated. Figure 10d shows the yield strength of specimens sintered by different sintering techniques versus different positions of the specimens. According to the figure, the yield strength of the specimens sintered by vacuum sintering and capsule HIP increases from center to periphery, corresponding to the slope of 7.3 and 7.4, respectively. This means the yield strength changed slightly from center to periphery of the specimens. This could have resulted from the uniform microstructure at all positions of the two mentioned specimens. In contrary, the yield strength of the specimens sintered by capsule-free HIP has an obvious rise from the center to the periphery with a slope of 52.5. This is nearly 7.2 times higher than that of the specimens sintered by vacuum sintering and capsule HIP techniques. The significant increase in yield strength is attributed to the increase in the relative density from the center to periphery of the specimens as discussed in the previous section.

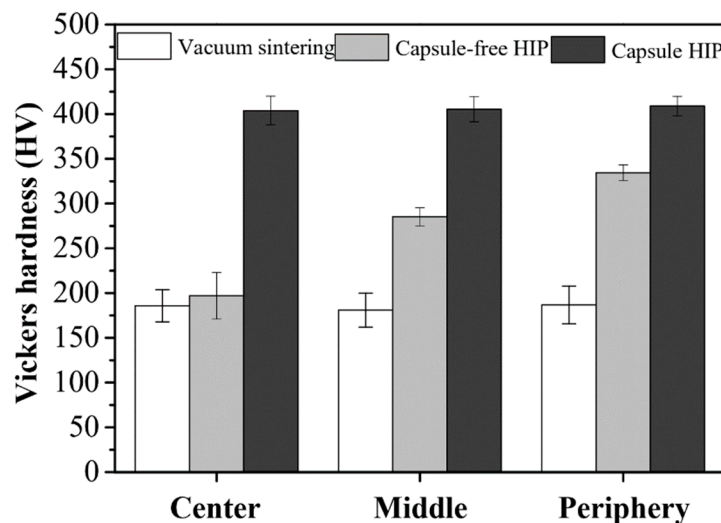


Figure 9. Vickers hardness of Ti6Al4V alloy sintered by different sintering techniques versus different positions of the specimens.

Several models based on Gibson and Ashby power law are usually used to estimate the effect of the relative density on the mechanical properties of Ti6Al4V alloy [27–29]. The models take into account some parameters such as the shape, size, and volume fraction of the pore, etc. However, these parameters are hardly assessed and thus the models usually work for a specific proposed system. Two common models are expressed by the Equations (1) and (2) for yield strength (σ_{ys}) as the following:

$$\frac{\sigma}{\sigma_o} = C\rho^{3/2}(1 + \rho^{1/2}) \quad (1)$$

$$\frac{\sigma}{\sigma_o} = (\rho)^n \quad (2)$$

$$\frac{\sigma}{\sigma_o} = 0.32 + 3.19 \times 10^{-4} \exp(0.08 * \rho) \quad (3)$$

where σ is the measured yield strength, σ_o (≈ 1070 MPa [30]) is defined as theoretical compressive yield strength, and C is constants of proportionality [29]. Figure 10e plots the normalized experimental yield strength against relative density. The best fitting data gave by Equation (1) with $C = 0.5$ still overestimate the experimental ones. This could be attributed that the model mainly validates for the porous materials having a relative density below 0.5 [30]. Fitting the data to the model expressed by Equation (2) gives a relationship with an exponent of 3.5. The calculated values are well fitted with the experimental data for the yield strength of the specimens sintered by vacuum sintering and capsule HIP. It is noted that the values obtained from Equation (2) still slightly higher than some reported experimental values [6,19]. In term of this, we proposed a new correction given by Equation (3).

The calculated values estimated from Equation (3) are a good match not only with reported values but also with the experimental values of the specimens sintered by vacuum sintering and capsule HIP. However, it is interesting to note that the measured yield strengths of the specimen sintered by capsule-free HIP at all positions are still significantly lower than those of the calculated data given by three equations. This was attributed to the coarse lamellar microstructure of α -Ti of the specimens consolidated by capsule-free HIP that caused the reduction in the yield strength compared to other techniques.

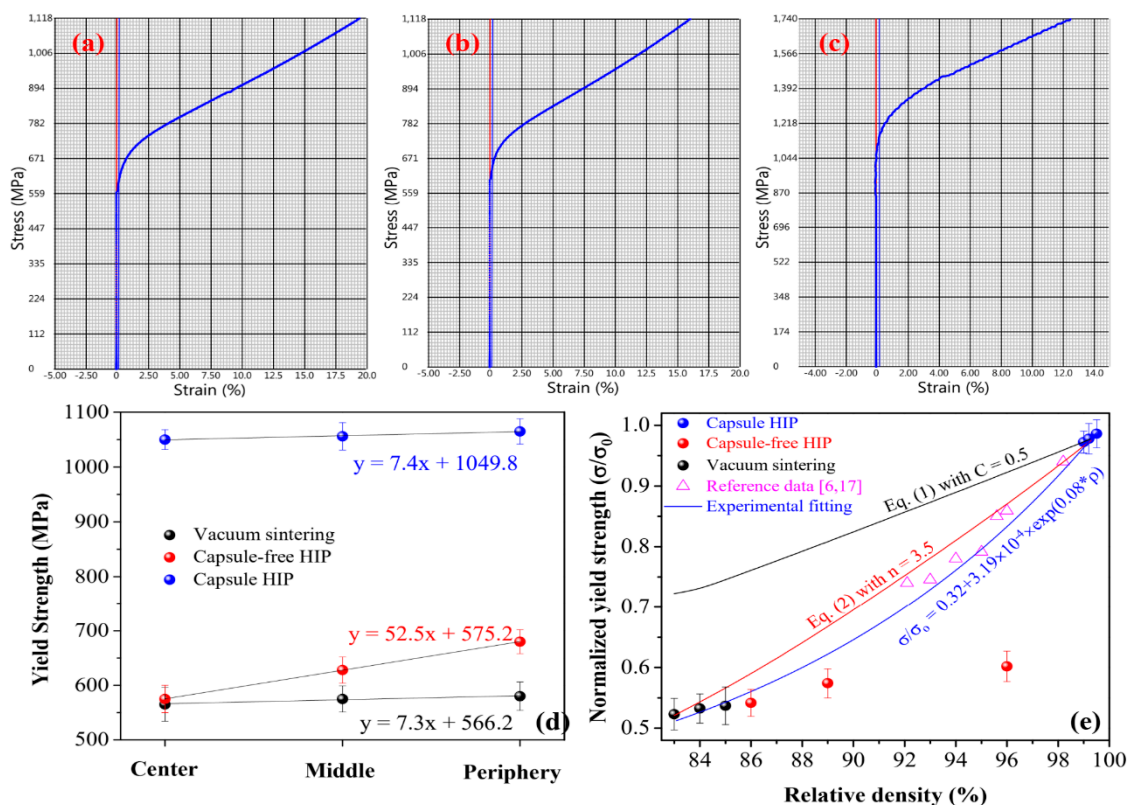


Figure 10. True stress–strain compression curves at middle position of Ti6Al4V alloy sintered by different techniques (a) vacuum sintering, (b) capsule-free HIP, and (c) capsule HIP, and (d) yield strength of Ti6Al4V alloy versus different positions of the specimens and (e) normalized yield strength of Ti6Al4V alloy sintered by different techniques as a function of the relative density.

4. Conclusions

We have investigated the microstructure and mechanical properties of Ti6Al4V alloy sintered by vacuum sintering, capsule-free HIP, and capsule HIP. The capsule HIP was the best technique to prepare the full density Ti6Al4V. The relative density and mechanical properties of the specimen sintered by capsule-free HIP are significantly influenced by the geometry. The relative density, hardness, and compressive yield strength rise from center to periphery due to the better densification at outside part than the inner part of the specimen. The calculated results indicated that the experimental yield strength of the specimen prepared by capsule-free HIP is much lower than that of the calculated values due to the coarse lamellar microstructure of α -Ti grains.

Author Contributions: Conceptualization, D.D.P. and P.V.T.; methodology, L.V.D. and N.V.L.; validation, P.V.T. and N.N.A.; investigation, L.V.D. and N.N.A.; writing—original draft preparation, L.V.D. and P.V.T.; writing—review and editing, D.D.P. and P.V.T.

Funding: This research was funded by Vietnam Academy of Science and Technology, grant number VAST.HTQT.BELARUS.03/17-18.

Acknowledgments: The authors acknowledge the support of the Vietnam Academy of Science and Technology under the project coded VAST.HIQT.BELARUS.03/17-18.

Conflicts of Interest: The authors declare no conflict of interest.

References

1. Norgate, T.E.; Wellwood, G. The potential applications for titanium metal powder and their life cycle impacts. *JOM* **2006**, *58*, 58–63. [[CrossRef](#)]
2. Froes, F.H.; Friedrich, H.; Kiese, J.; Bergoint, D. Titanium in the family automobile: The cost challenge. *JOM* **2004**, *56*, 40–44. [[CrossRef](#)]
3. Sen, I.; Tamirisakandala, S.; Miracle, D.B.; Ramamurty, U. Microstructural effects on the mechanical behavior of B-modified Ti–6Al–4V alloys. *Acta Mater.* **2007**, *55*, 4983–4993. [[CrossRef](#)]
4. Singh, G.; Sen, I.; Gopinath, K.; Ramamurty, U. Influence of minor addition of boron on tensile and fatigue properties of wrought Ti-6Al-4V alloy. *Mater. Sci. Eng. A* **2012**, *540*, 142–151. [[CrossRef](#)]
5. Banerjee, D.; Williams, J.C. Perspectives on titanium science and technology. *Acta Mater.* **2013**, *61*, 844–879. [[CrossRef](#)]
6. Yan, Z.Q.; Chen, F.; Cai, Y.X.; Jian, Y.N. Influence of particle size on property of Ti-6Al-4V alloy prepared by high-velocity compaction. *Trans. Nonferrous Met. Soc. China* **2013**, *23*, 361–365. [[CrossRef](#)]
7. Yan, Y.J.; Nash, G.L.; Nash, P. Effect of density and pore morphology on fatigue properties of sintered Ti-6Al-4V. *Int. J. Fatigue* **2013**, *55*, 81–91. [[CrossRef](#)]
8. Ng, H.P.; Haase, C.; Lapovok, R.; Estrin, Y. Improving sinterability of Ti-6Al-4V from blended elemental powders through equal channel angular pressing. *Mater. Sci. Eng. A* **2013**, *565*, 396–404. [[CrossRef](#)]
9. Torres, Y.; Rodríguez, J.A.; Arias, S.; Echeverry, M.; Robledo, S.; Amigo, V.; Pavón, J.J. Processing, characterization and biological testing of porous titanium obtained by space-holder technique. *J. Mater. Sci.* **2012**, *47*, 6565–6576. [[CrossRef](#)]
10. Long, Y.; Zhang, H.Y.; Wang, T.; Huang, X.L.; Li, Y.Y.; Wu, J.S.; Chen, H.B. High-strength Ti-6Al-4V with ultrafine-grained structure fabricated by high energy ball milling and spark plasma sintering. *Mater. Sci. Eng. A* **2013**, *585*, 408. [[CrossRef](#)]
11. Xu, L.; Guo, R.P.; Bai, C.G.; Lei, J.F.; Yang, R. Effect of hot isostatic pressing conditions and cooling rate on microstructure and properties of Ti-6Al-4V alloy from atomized powder. *J. Mater. Sci. Technol.* **2014**, *30*, 1289. [[CrossRef](#)]
12. Murr, L.E.; Esquivel, E.V.; Quinones, S.A.; Gaytan, S.M.; Martinez, E.Y.; Medina, F.; Hernandez, D.H.; Martinez, E.; Martinezl, J.L.; Stafford, S.W.; et al. Microstructures and mechanical properties of electron beam-rapid manufactured Ti-6Al-4V biomedical prototypes compared to wrought Ti-6Al-4V. *Mater. Charact.* **2009**, *60*, 96–105. [[CrossRef](#)]
13. Zhang, L.C.; Attar, H.; Calin, M.; Eckert, J. Review on manufacture by selective laser melting and properties of titanium based materials for biomedical applications. *Mater. Technol.* **2016**, *31*, 66–76. [[CrossRef](#)]
14. Zhang, L.C.; Liu, Y.; Li, S.; Hao, Y. Additive manufacturing of Titanium alloys by electron beam melting: A review. *Adv. Eng. Mater.* **2018**, *20*, 1700842. [[CrossRef](#)]
15. German, R.M. *Sintering Theory and Practice*; John Wiley and Sons: New York, NY, USA, 1996; p. 100.
16. Bayat, H.; Rastgo, M.; Zadeh, M.M.; Vereecken, H. Particle size distribution models, their characteristics and fitting capability. *J. Hydrol.* **2015**, *529*, 872–889. [[CrossRef](#)]
17. Razavi-Tousi, S.S.; Yazdani-Rad, R.; Manafi, S.A. Effect of volume fraction and particle size of alumina reinforcement on compaction and densification behavior of Al-Al₂O₃ nanocomposites. *Mater. Sci. Eng. A* **2011**, *528*, 1105–1110. [[CrossRef](#)]
18. Xu, X.Y.; Nash, P. Sintering mechanisms of Armstrong prealloyed Ti-6Al-4V powders. *Mater. Sci. Eng. A* **2014**, *607*, 409. [[CrossRef](#)]
19. Cabezas-Villa, J.L.; Lemus-Ruiz, J.; Bouvard, D.; Jiménez, O.; Vergara-Hernández, H.J.; Olmos, L. Sintering study of Ti6Al4V powders with different particle sizes and their mechanical properties. *Int. J. Miner. Metall. Mater.* **2018**, *25*, 1389–1401. [[CrossRef](#)]
20. Baccino, R.; Morret, F.; Fellerin, F.; Guichard, D.; Raison, G. High performance and high complexity net shape parts for gas turbines: the ISOPREC® powder metallurgy process. *Mater. Des.* **2000**, *21*, 345–350. [[CrossRef](#)]

21. Mashl, S.J.; Hebeisen, J.C.; Hjorth, C.G. Producing large P/M near-net shapes using hot isostatic pressing. *JOM* **1999**, *7*, 29–31. [[CrossRef](#)]
22. Froes, F.H.; Mashl, S.J.; Hebeisen, J.C.; Moxson, V.S.; Duz, V.A. The technologies of titanium powder metallurgy. *JOM* **2004**, *56*, 46–48. [[CrossRef](#)]
23. Atkinson, H.V.; Davies, S. Fundamental aspects of hot isostatic pressing: An overview. *Metall. Mater. Trans. A* **2000**, *31*, 2981–2987. [[CrossRef](#)]
24. Delo, D.P.; Piehler, H.R. Early stage consolidation mechanisms during hot isostatic pressing of Ti-6Al-4V powder compacts. *Acta Mater.* **1999**, *47*, 2841–2852. [[CrossRef](#)]
25. Zhang, K.; Mei, J.; Wain, N.; Wu, X. Effect of hot-isostatic-pressing parameters on the microstructure and properties of powder Ti-6Al-4V hot-isostatically-pressed samples. *Metall. Mater. Trans. A* **2010**, *41*, 1033–1045. [[CrossRef](#)]
26. Trinh, P.V.; Luan, N.V.; Phuong, D.D.; Minh, P.N.; Weibel, A.; Mesguich, D.; Laurent, C. Microstructure, microhardness and thermal expansion of CNT/Al composites prepared by flake powder metallurgy. *Composites Part A* **2018**, *105*, 126–137. [[CrossRef](#)]
27. Ashby, M.F. The properties of foams and lattices. *Philos. Trans. R. Soc. Ser. A* **2006**, *364*, 15–30. [[CrossRef](#)] [[PubMed](#)]
28. Gibson, L.J.; Ashby, M.F. *Cellular Solids: Structure and Properties*; Cambridge University Press: Cambridge, UK, 1999; p. 52.
29. Hernandez-Nava, E.; Smith, C.J.; Derguti, F.; Tammam-Williams, S.; Léonard, F.; Withers, P.J.; Todd, I.; Goodalla, R. The effect of density and feature size on mechanical properties of isostructural metallic foams produced by additive manufacturing. *Acta Mater.* **2015**, *85*, 387–395. [[CrossRef](#)]
30. ASM Handbook Committee, American Society for Metals. *Properties and Selection: Stainless Steels, Tool Materials and Special-Purpose Metals*, 9th ed.; ASM International: Materials Park, OH, USA, 1980; p. 388.



© 2019 by the authors. Licensee MDPI, Basel, Switzerland. This article is an open access article distributed under the terms and conditions of the Creative Commons Attribution (CC BY) license (<http://creativecommons.org/licenses/by/4.0/>).